Part I
Gas Phase

Methods in Physical Chemistry, First Edition. Edited by Rolf Schäfer and Peter C. Schmidt.

1
Manipulating the Motion of Complex Molecules: Deflection, Focusing, and Deceleration of Molecular Beams for Quantum-State and Conformer Selection[1)]

Jochen Küpper, Frank Filsinger, Gerard Meijer, and Henrik Stapelfeldt

Method Summary

Acronyms

- Effective dipole moment (μ_{eff})
- Low-field-seeking (lfs) state
- High-field-seeking (hfs) state
- Alternating gradient (AG) focusing
- Transition state (TS).

Benefits (Information Available)

- allows one to spatially separate molecules in different quantum states, including isomers of complex molecules
- versatile – DC field techniques can be applied to all polar molecules, AC field techniques to all polarizable molecules (= all molecules)
- quantum-state specific interaction – can, in principle, be used to separate all kinds of isomers
- determination of rotational, vibrational, and electronic properties – including dipole moments and polarizabilities – of single isomers of complex molecules
- allows detailed investigations of stereochemical dynamics
- allows one to separate molecular ensembles from seed gas, avoiding background in various scattering experiments.

Limitations (Information Not Available)

- translations of non-polar molecules can – for practical purposes – not be manipulated by DC electric fields
- no ultracold samples (μK or below) produced so far.

1) This chapter is largely based on parts of Ref. [1].

Methods in Physical Chemistry, First Edition. Edited by Rolf Schäfer and Peter C. Schmidt.

1.1 Introduction: Controlled Molecules

Chemists have long been dreaming of ultimately controlling all aspects of chemical reactions. Empirically, vast progress has been made over the last centuries using increasingly sophisticated techniques to dictate the path and outcome of chemical reactions. However, in all these approaches external parameters are used to (classically) shift statistical outcomes one way or another. Recently, the field of cold and ultracold chemistry has started to provide a glimpse at a new level of control, where full quantum-mechanical control can be obtained. So far this has been demonstrated for very specific small reaction systems, that is, for reactions of alkali dimers with alkali atoms [2, 3] or with each other, including the observation of stereochemical effects [4]. In these experiments molecules are prepared at low temperatures and specific quantum states starting from ultracold ensembles of, typically, alkali atoms, which is the limiting factor to the possible complexity and versatility of these methods. Alternatively, cold collisions of small molecules, that is, OH radicals, with rare gas atoms at arbitrarily low collision energies have been investigated [5, 6]. In this chapter we will present the available methods to gain control over the motion and the quantum-state populations of complex molecules (albeit at a lower level). These methods could enable a new level of detail in the study and control of chemical reactions for a large variety of molecules.

Moreover, the prepared samples of controlled molecules are useful in a wide variety of experiments, ranging from the taking of actual photographs of the molecules – and their inherent or induced dynamics – using ultrafast X-ray or electron diffraction [1] over, for example, photoelectron distributions and high-harmonic generation to investigations of attosecond electron dynamics and charge migration [7]. These experiments would provide direct information on the occurring chemical dynamics through imaging of the nuclear geometry and the electronic wavefunctions.

1.2 Experimental Methods

In this section we will first summarize experiments to prepare cold supersonic jets of complex molecules and then describe methods to manipulate the motion of complex molecules in a molecular beam.

Box 1.1 Molecular Beams

Molecular beams are formed by expanding a gas from a reservoir at high pressure through a small orifice into vacuum, as shown schematically in Figure 1.1 [61, 126, 146]. Thus, in principle, a molecular beam is nothing but a "leak in a vacuum system," as John B. Fenn called it [146]. Molecular beams are called

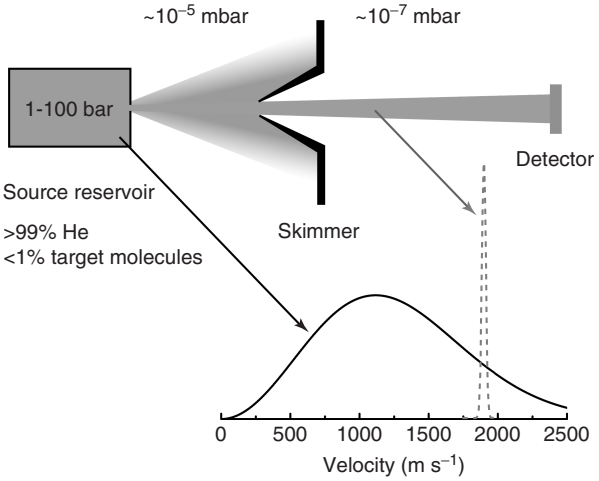

Figure 1.1 A molecular beam is formed by expanding gas-phase molecules seeded in a noble gas from a reservoir at high pressure into vacuum. Often the molecular beam is collimated using a skimmer, which also allows differential pumping, separating the source chamber from the detection chamber. Typical velocity distributions in the source region (black) and in the molecular beam (dotted gray) are shown, as obtained when using room-temperature He as the carrier gas.

effusive if the orifice diameter is much smaller than the mean free path of the gas in the high-pressure reservoir. In this case, the molecules can escape from the reservoir without undergoing collisions and the velocity distribution and the quantum-state population in the molecular beam is the same as in the source region. If, on the other hand, the pressure in the container is increased or the size of the orifice is decreased so that the mean free path in the source becomes smaller than the orifice diameter, molecules passing through the hole will collide frequently during their ''escape.'' These collisions convert a large fraction of the total energy that is available per molecule into kinetic energy along the molecular beam axis, resulting in a highly directed flow. In other words, in such so-called supersonic beams, the molecules' internal (i.e., rotational and vibrational) degrees of freedom are adiabatically cooled. Cooling only takes place within a short distance from the orifice where the particle densities are still high enough to allow frequent collisions. Once these collisions have stopped, a few centimeters downstream from the orifice, the terminal temperature is reached. This terminal temperature is limited by the formation of clusters, which typically is minimized to an acceptable level by diluting the molecules to be investigated with an inert carrier gas (typically a noble gas) before the expansion. Translational and rotational temperatures below 1 K can be reached in supersonic beams, whereas vibrational temperatures are usually somewhat

higher. The terminal velocity of the molecular beam is determined by the mass of the carrier gas, the source temperature and the source pressure. The dotted gray trace in Figure 1.1 shows a typical velocity distribution for molecules seeded in He at room temperature. Here, the mean velocity is about 1900 m s^{-1}. Molecular beams can be operated in continuous or pulsed mode. Typically, pulsed beams yield higher particle densities, because pumping requirements are less severe and, therefore, larger orifices and higher stagnation pressures can be used. They are well suited for inherently pulsed experiments, that is, when using pulsed lasers for detection. In pulsed beams, densities of 10^{13} molecules cm^{-3} can be reached for small molecules like ammonia or CO. The densities for larger molecules are typically a few orders of magnitude smaller.

1.2.1
Large Neutral Molecules in the Gas Phase

During the last decades, the properties of neutral complex (bio-) molecules in the gas phase, that is, in molecular beams, have been studied in ever greater detail [8–10]. Although the study of biomolecules outside of their natural environment was initially met with skepticism, spectroscopic studies on isolated species in a molecular beam have proven to be very powerful for understanding the molecules' intrinsic properties and for benchmarking theoretical calculations. Moreover, the molecule's native environment can be partly mimicked by adding solvent molecules one by one [10–12]. Even in the cold environment (∼1 K) of a molecular beam, biomolecules exist in various conformational structures [13, 14], see Box 1.2. In many cases, the individual conformers are identified via their different electronic spectra [14, 15]. Structural information on the individual conformers can be deduced from, for instance, multiple-resonance techniques, which yield conformer-specific infrared spectra [16, 17], from the different angles between vibrational transition moments and the permanent dipole moments of oriented molecules [18], the different quadrupole coupling constants, determined by means of Fourier-transform microwave spectroscopy [19], or the different permanent dipole moments, deduced from the rotationally resolved spectra [20, 21]. Apart from this information on the local minima on the potential energy surface, information on the barriers separating the conformers has been obtained in sophisticated multiple-resonance experiments [22].

For many experiments in chemistry and physics, however, it is desirable to spatially separate the individual conformers, or structural isomers in general. Such conformer-selected samples are expected to benefit a variety of future applications such as tomographic imaging experiments [23] or ultrafast dynamics studies on the ground-state potential energy surface. For ultrafast electron and X-ray diffraction experiments [24–26] aiming at the ''molecular movie,'' that is, measuring chemical processes with spatial and temporal atomic resolution (a few picometers and femtoseconds, respectively) the preparation of conformer-selected samples might be crucial.

For charged species, the separation of structurally different molecules has been performed using ion mobility in drift tubes [27, 28]. For neutral molecules it has been demonstrated that the abundance of the conformers in the beam can be partly influenced by selective over-the-barrier excitation in the early stage of the expansion [29] or by changing the carrier gas [30]. These methods are, however, neither generally applicable nor able to specifically select individual conformers. Below, we describe the preparation of conformer-selected samples of complex molecules using electric fields.

Box 1.2 Quantum-Level Structure and Structural Isomers of Large Molecules

The potential-energy surface of complex molecules exhibits many local minima that correspond to distinct conformational structures, as schematically shown in Figure 1.2a. Even at the low temperatures that can be reached in supersonic expansions (see Box 1.1), not only the global minimum of the electronic-ground-state surface but also many of these local minima are populated. The relative populations of the various conformers are determined both

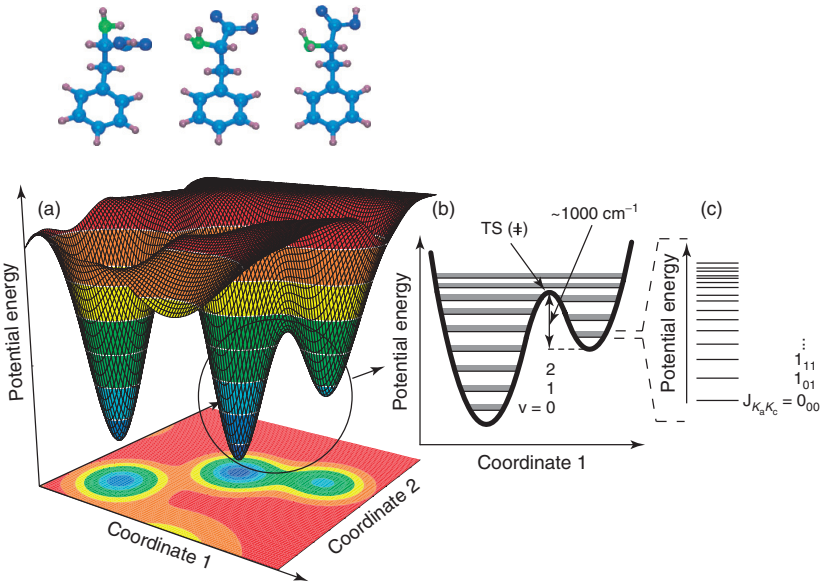

Figure 1.2 (a) The ground-state potential energy surface of complex molecules exhibits many local minima, corresponding to different conformers, and with distinct transition states (TSs) connecting the minima. (b) Each conformer has a distinct vibrational level scheme. (c) Each vibrational level has a rotational substructure.

by the experimental conditions during the expansion (for instance, the type of carrier gas, the stagnation pressure, and the type of nozzle that is used) and by the potential energy landscape. Typical barriers separating the local minima are of the order of 1000 cm^{-1}. These barriers are too high for thermally induced conformational change to occur under the cold conditions in a molecular beam. The conformational distribution in a molecular beam is thus ''frozen'' and the individual conformers, which exhibit distinct vibrational level structures as shown in Figure 1.2b, are typically all in their vibrational ground state (or in a few low-lying vibrational states). A molecule in a given vibrational state can be in many different rotational states, as indicated in Figure 1.2c. Due to the small rotational constants of large molecules the density of rotational states is high and the population is often distributed over many (thousands of) rotational states even, at rotational temperatures of a few K. The field-free rotational states of asymmetric top molecules are labeled by J_{KaKc}, where J is the total angular momentum quantum number and K_a and K_c are two pseudo-quantum numbers that link the asymmetric rotor states to the limiting prolate and oblate symmetric top quantum states [147]. Under field-free conditions each $J_{K_aK_c}$-state is $(2J + 1)$-fold degenerate. This degeneracy is lifted by an electric field, which splits the field-free states into $(J + 1)$-sublevels according to the quantum number M, which corresponds to the projection of the total angular momentum onto the field axis (see Box 1.3).

1.2.2 Manipulation of Molecular Beams with Electric and Magnetic Fields

1.2.2.1 Deflection of Polar Molecules

A century ago, when molecular beams were initially investigated [31], today's sophisticated laser-based quantum-state-selective detection techniques were still lacking. In 1921, Stern proposed that the trajectories of silver atoms on their way to the detector could be characteristically altered, depending on their quantum state, when the atomic beam was exposed to an inhomogeneous magnetic field [32]. In a ground-breaking experiment, Gerlach and Stern demonstrated in 1922 [33] that, indeed, quantum-state selectivity could be achieved in the detection process by sorting different quantum states *via* space quantization, a concept that has been extensively used ever since. The possibility to deflect polar molecules in a molecular beam with electric fields was conceived at the same time. It was first described theoretically by Kallmann and Reiche in 1921 [34][2)] and later demonstrated experimentally by Wrede – a graduate student of Stern – in 1927 [35].

2) In fact, Stern states in a footnote to his original paper on space quantization [32] that its publication was motivated by Kallmann and Reiche's article, of which he had received the galley proofs.

As early as 1926, Stern suggested that the technique could be used for the quantum-state separation of small diatomic molecules at low temperatures [36]. Over the years, various experimental geometries were designed to create strong field gradients on the beam axis in order to efficiently deflect particles. In 1938/1939 Rabi introduced the molecular beam magnetic resonance method, using two deflection elements of oppositely directed gradients in succession, to study the quantum structure of atoms and molecules [37, 38]. In his setup, the deflection of particles caused by the first magnet was compensated by a second magnet such that the particles reached the detector on a sigmoidal path. If, between the two magnets, a transition to a different quantum state was induced, this compensation was incomplete and a reduction in the detected signal could be observed. Since these early days of molecular beam deflection experiments, the deflection technique has been widely used as a tool to determine dipole moments and polarizabilities of molecular systems ranging from diatomics [35] to clusters [39, 40] and large biomolecules [41]. Recently, the possibility to separate structural isomers of complex molecules by electric deflection was demonstrated [42].

Box 1.3 Manipulation of Polar Molecules *via* the Stark Effect

Neutral molecules interact with electric fields through their charge distribution, an effect called the *Stark effect*. For polar molecules in DC electric fields this is practically solely due to the interaction of the molecular electric dipole moment μ with the electric field. A homogeneous electric field can be used to orient polar molecules as depicted schematically in Figure 1.3a (see also Box 1.4). There is no net force on the oriented molecule in this case as the potential energy is spatially constant. In an inhomogeneous field, however, the situation shown in Figure 1.3b, there is a spatial variation of the potential energy, resulting in a net force, simply because every physical system tries to minimize its energy. This can be utilized to manipulate the molecule's motion by appropriately shaped electric fields.

Quantum-mechanically the dipole operator couples different molecular states, equivalent to the coupling of states by the light field in an optical transition. The DC Stark effect couples states with opposite parity that differ by one in J and that have the same M quantum number, where J is the total angular momentum, m_J its projection on the field axis and $M = |m_J|$. In Figure 1.3 the calculated energies for a few of the lowest rotational states of benzonitrile (C_7H_5N) are shown. These curves are obtained by setting up the Hamiltonian matrix based on the known matrix elements [149] and spectroscopically obtained rotational constants and dipole moments [148]. From Figure 1.3 it is obvious that for all quantum states of benzonitrile the energy decreases with increasing field strength for practically relevant electric fields (50–200 kV cm^{-1}) and these states are called high-field-seeking. This is typical for ''large molecules'', whereas for ''small molecules'' with large rotational constants low-field-seeking states with

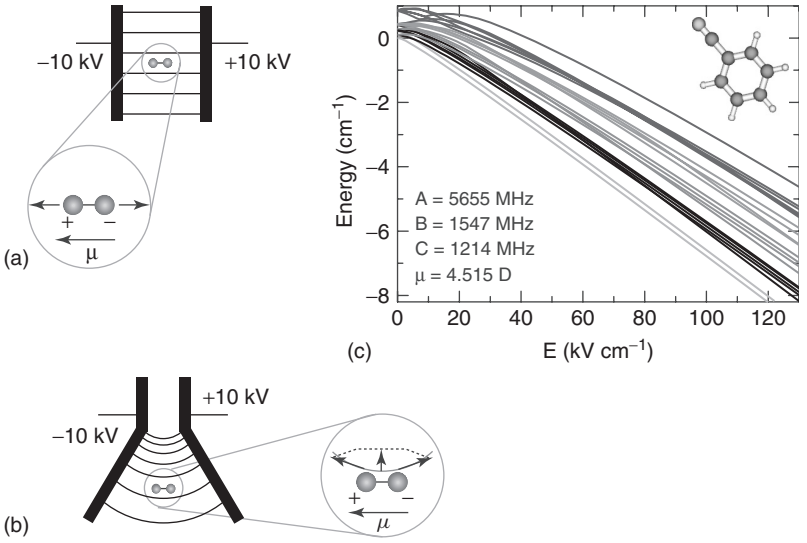

Figure 1.3 (a) Homogeneous electric fields can be used to orient polar molecules. The field does not provide an overall (translational) force on the molecule, but it provides a torque to orient the molecular dipole moment along the electric field lines. (b) Inhomogeneous electric fields exert a force on polar molecules: the centers of positive and negative charge do not coincide and, therefore, the forces on these charge-centers do not cancel exactly. Instead, a small remaining force, depicted by the vectorial sum in the inset, remains and can be used to manipulate the translation of the molecule. (c) Potential energy as a function of the electric field strength for the lowest rotational quantum states of benzonitrile. These energies can be calculated from the spectroscopically determined rotational constants A, B, C and the dipole moment μ [147].

the opposite behavior are observed [46]. Moreover, the lowest states are the most polar ones. In simple terms this can be understood by the fact that the lowest states are mostly repelled from a large number of states that are higher in energy and only from a very small set of states that are lower in energy. It is illustrative to introduce the effective dipole $\mu_{\mathrm{eff}} = -\mathrm{d}W/\mathrm{d}E$, which is the negative gradient of the Stark energy W with respect to the magnitude of the electric field, E. The force is obtained as $\vec{F} = -\vec{\nabla} W(E)$ which can then be expressed as $\vec{F} = \mu_{\mathrm{eff}}(E)\cdot\vec{\nabla} E$, that is, it is given by the effective dipole moment at the position and field of the molecule times the spatial gradient of the electric field. Because the effective dipole moment depends on the quantum state, inhomogeneous electric fields can be used to separate molecules in different quantum states, which is the basic concept behind the experimental techniques described in this chapter. In general, the lowest rotational quantum states have the largest μ_{eff} and experience the strongest force in an electric field.

1.2.2.2 Focusing and Deceleration of Molecules in Low-Field-Seeking Quantum States

Whereas deflection experiments allow the spatial dispersion of quantum states, they do not provide any focusing of the molecular beam. For small molecules in eigenstates whose energy increases with increasing field strength, so-called low-field-seeking (lfs) states, focusing was achieved using multipole focusers. Both magnetostatic [43, 44] and electrostatic [45] devices were developed in the early 1950s by Paul's group in Bonn. Independently, an electrostatic quadrupole focuser, that is, a symmetric arrangement of four cylindrical electrodes around the beam axis that are alternately charged by positive and negative high voltages, was built in 1954/1955 by Gordon, Zeiger and Townes in New York to create population inversion of ammonia molecules for the first demonstration of the maser [46, 47]. Using several multipole focusers in succession, and interaction regions with electromagnetic radiation in between them, many setups were developed to unravel the quantum structure of atoms and molecules – very similar to Rabi's molecular beam magnetic resonance method. About 10 years after the invention of the multipole focusing technique, molecular samples in a single rotational state were used for state-specific inelastic scattering experiments by the Bonn group [48] and, shortly thereafter, for reactive scattering studies [49, 50]. In the following decades, multipole focusers were extensively used to study steric effects in gas-phase reactive scattering experiments [51–53]. The preparation of oriented samples of state-selected molecules using electrostatic focusers was also essential for the investigation of steric effects in gas-surface scattering [54] and photodissociation [55] experiments. Variants of multipole focusing setups were implemented in many laboratories all over the world and yielded important information on stable molecules, radicals, and molecular complexes.

Finally, in 1999, the so-called Stark decelerator was realized [56], allowing the same control over the forward velocities of molecules in lfs states. This technique was used to confine small molecules in storage rings [57] and static [58] and dynamic traps [59]. Recently, the ''decelerator on a chip'' – a miniaturized version of the Stark decelerator – has been implemented [60]. Detailed accounts of the field of Stark deceleration have been given elsewhere [61–64].

1.2.2.3 Focusing and Deceleration of Molecules in High-Field-Seeking Quantum States

Large or heavy molecules have small rotational constants and, as a consequence, a high density of rotational states. Coupling between closely spaced states of the same symmetry turns lfs states into high-field-seeking (hfs) states already at relatively weak electric field strengths (compared to the field strengths that are required for efficient focusing). In order to focus molecules in these states, a maximum of the electric field in free space would have to be created. Since Maxwell's equations do not allow the creation of such a field with static fields alone [65, 66], static multipole fields cannot be applied to focus molecules in hfs states. The situation is analogous to charged particle physics: charged particles also cannot be confined with static fields alone. This focusing problem for ions was solved when Courant,

Livingstone, and Snyder introduced the principle of ''alternating gradient (AG) focusing'' in the 1950s [67, 68]. The basic idea is to create an array of electrostatic lenses that focus the particles along one transverse coordinate while defocusing them along the perpendicular transverse axis. Alternating the orientation of these fields at the appropriate frequency results in a net focusing force along both transverse coordinates. This principle is exploited to confine ions, for instance, in quadrupole mass filters [69, 70], in Paul traps [69, 70], and in virtually all particle accelerators. The application of AG focusing to neutral polar molecules was first proposed by Auerbach, Bromberg, and Wharton [72] and demonstrated experimentally by Kakati and Lainé for ammonia molecules in hfs states [73–75]. Later, the diatomic KF [76, 77] and ICl [78] molecules were also focused. More recently, slow ammonia molecules were guided from an effusive source using a bent AG focuser [79], but molecules in lfs and hfs states could not be distinguished because the detection process was not state selective. Furthermore, diatomic CaF molecules have been guided using a 1-m-long straight AG focuser [80]. Recently, the rotational-quantum-state specific guiding of the prototypical large molecule benzonitrile has been the subject of detailed analysis [81]. Besides the AG focusing technique using switched electric fields, various alternative approaches have been implemented to focus molecules in hfs states, such as exploiting the fringe fields of ring-like electrode structures [82], the fields created by crossed wires [83], or the fields created by coaxial electrodes [84–87]. Most of these methods, however, were only used for proof-of-principle experiments and did not find further applications.

The first attempt to manipulate the forward velocity of molecules in hfs states was reported in the 1960s, when the group of Wharton at the University of Chicago set up an 11-m-long machine to accelerate LiF molecules [88, 89]. Similarly, Golub and King had set up a decelerator for ammonia molecules at MIT [90]. While these early experiments were unsuccessful and stopped after the PhD student had finished his thesis, a decelerator design that exploits the AG principle for transverse confinement of the molecules was successfully implemented in 2002 [91], inspired by the successful deceleration of small molecules with the Stark decelerator. So-called AG decelerators were used to decelerate CO [91, 92], YbF [93], and benzonitrile [94] molecules in hfs quantum states and OH radicals in both hfs and lfs states [95, 96]. In these first experiments on hfs molecules, up to 30% of the kinetic energy was removed, but so far it has not been possible to decelerate molecules to velocities that are small enough for trapping in stationary traps. However, AC trapping of para-ND3 in the hfs component of its ground rotational state ($J_K = 1_1$) was achieved by decelerating the molecule in a lfs state with a conventional Stark decelerator and subsequently transferring the population to the hfs state using microwave radiation [59, 97].

1.2.2.4 **Electromagnetic High-Frequency AC Fields**

Electromagnetic high-frequency AC fields have also been used for the deflection, focusing, and deceleration of neutral molecules, and these methods are generally applicable to molecules in all, dc lfs and hfs, states. Strong laser fields have been

used to deflect and focus [98, 99] and to decelerate [100] a fraction of the molecules in a beam. Alternatively, the deceleration of molecules using microwave fields has been proposed [101] and the transverse focusing of molecules with microwave fields has been demonstrated [102].

1.2.3 Alignment and Orientation of Molecular Ensembles

Whereas this chapter focuses on the manipulation of the translational motion of molecules, methods to manipulate the rotational motion, that is, to create aligned or oriented ensembles of molecules, have also been demonstrated. There are several electric-field-based methods that are applicable for large molecules, which are generally asymmetric rotors. The conceptually simplest method to confine the angular distribution of polar molecules is the interaction of the molecular dipole with a strong homogeneous electric field, as proposed independently by Loesch and Remscheid [103] and by Friedrich and Herschbach [104]. This ''brute force orientation'' has been demonstrated experimentally many times and is summarized elsewhere [105, 106]. It has been exploited, for example, to determine transition moment angles in the molecular frame [18, 107]. For molecules in low-field-seeking states, orientation is naturally achieved through state-selection in multipole focusers [52, 53, 108, 109].

Applying strong, non-resonant laser fields to the molecules also provokes angular confinement [110]. In order to achieve the necessary field strength, typically, pulsed lasers are employed. Depending on the laser pulse duration the confinement is achieved adiabatically – when the laser pulse is long compared to the molecules' rotational period, or impulsively – when the laser pulse is short compared to the molecules' rotational period. In the latter case field-free alignment is achieved at the revivals obtained after the kick pulse. For a more-in-depth discussion of alignment and orientation the reader is referred to the existing excellent reviews [110, 111].

Whereas the laser field can only create alignment, both approaches – adiabatic and impulsive laser–molecule interactions – have been used to obtain orientation by adding small DC electric fields, as suggested by Friedrich and Herschbach [112, 113]. Recently, strong alignment and orientation by mixed DC electric and laser fields has been demonstrated for linear molecules [114–118] and even for large asymmetric top molecules [119–122]. The crucial influence of the population of rotational states on the achievable alignment has been investigated experimentally [123]. Clearly, the state selection of the lowest rotational states, for example, performed by the experiments described in this chapter, allows considerably stronger degrees of alignment and orientation.

Box 1.4 Alignment and Orientation

Alignment is an order of the molecular geometry with respect to a space fixed axis, whereas for orientation a direction with respect to the space fixed axis is also defined, that is, the inversion symmetry with respect

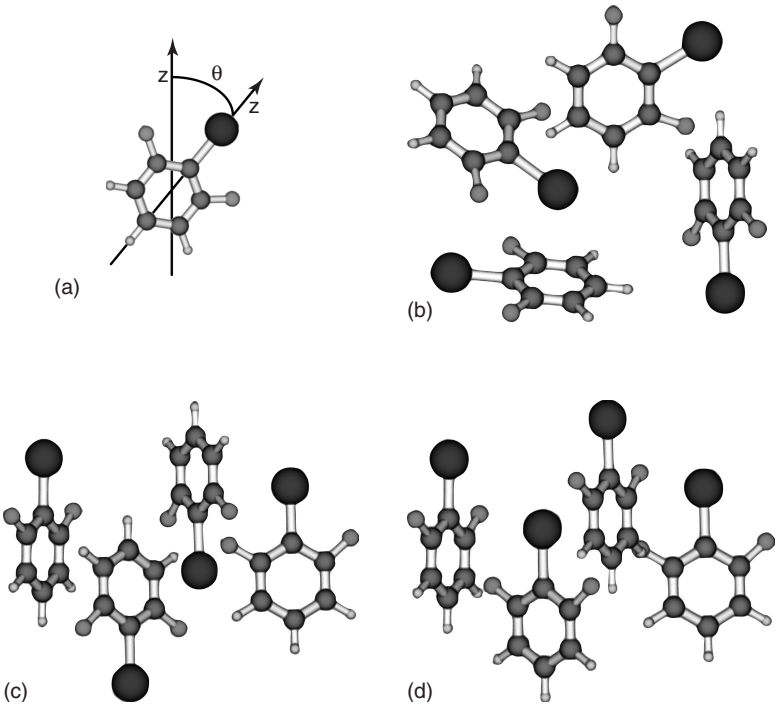

Figure 1.4 Depiction of (one-dimensional) alignment and orientation of a molecular ensemble. (a) Definition of θ as the angle between a molecule-fixed and a space-fixed axis, that is, the most polarizable axis of the molecule and the direction of the field, respectively. (b) In an isotropic sample no order regarding the space fixed axis – or θ – exists. (c) In an aligned sample all molecules have θs close to 0 or π, for an oriented sample all molecules have θs close to 0 (d).

to the space-fixed axis is broken. This is depicted in Figure 1.4. The distribution of θs for the ensemble of molecules can be described as a series of Legendre polynomials, which is typically truncated after the squared term: $P(\theta) = 1 + a_1 P_1(\cos\theta) + a_2 P_2(\cos\theta) + \ldots$ and the anisotropy is described by the Legendre moments $\langle\cos\theta\rangle$ and $\langle\cos^2\theta\rangle$. These terms have values 0 and 1/3 for an isotropic sample (Figure 1.4b), and $> 1/3$ for an aligned sample (Figure 1.4c), and > 0 and $> 1/3$ for an oriented sample (Figure 1.4d).

As mentioned in Box 1.3, an electric field not only exerts a force on a molecule regarding the translations, but also regarding the rotations. A DC electric field leads to orientation of the (effective) dipole moment along the field lines. In a homogeneous field all quantum states of large molecules (*vide supra*) will be oriented along the same axis – the field axis.

Alternatively, one can align molecular ensembles using high-frequency AC electric fields, that is, laser fields [110]. While the dipole of a polar molecule

is fixed in the molecular frame and cannot follow the fast oscillation of the high-frequency AC field, the molecular polarizability leads to an AC Stark shift. If the polarizabilities along the principal axes of the molecule are not equal, this will again lead to a angular force on the molecule in the field, aligning the molecules with their most-polarizable axis along the polarization axis of the field. However, since the AC field does not have directionality, it cannot induce orientation. Adding (small) DC electric fields can overcome this limitation, resulting in so-called mixed-field orientation [112, 117, 119]. However, while one can only create one-dimensional orientation with a DC field alone, an elliptically polarized laser field allows one to induce three-dimensional alignment [138] and orientation [120].

One successful experimental approach to observe the degree of alignment and orientation of a molecular ensemble is Coulomb explosion imaging, see Figure 1.10. The molecules are multiply ionized using a short (<50 fs) laser pulse, resulting in Coulomb repulsion of the different (positively) charged parts of the molecule. If this results in a charged atom dissociating from the molecule along a well-defined molecular axis (the ''axial-recoil approximation''), it is a direct measurement of the orientation of the molecules before ionization. For example, the distribution of iodine cations in Figure 1.10 is a direct measurement of the C–I bond axis of the iodobenzene molecules before ionization.

1.3 Experimental Details

1.3.1 Deflection

A schematic of the experimental setup for electric deflection is shown in Figure 1.5, depicting the general theme of the experimental setups for manipulating the motion of molecules in supersonic cold molecular beams. The molecular beam machine consists of three differentially pumped vacuum chambers; the source chamber housing a pulsed valve, the deflector chamber, and the detection chamber housing the ion/electron spectrometer. Some mbar of the investigated molecules are seeded in an inert carrier gas, that is, rare gases, and expanded through a pulsed valve into vacuum. In order to obtain optimal cooling of the molecular beam, a high-pressure Even–Lavie solenoid valve [124] is used, operating at a backing pressure of 90 bar of He or 20 bar of Ne, limited by the onset of cluster formation. While rotational temperatures down to 0.4 K have been achieved under similar conditions [125], the typical terminal rotational temperature from the expansions in our experiments is ~1 K. Two 1-mm-diameter skimmers placed 15 cm (separating the source and the deflector chamber) and 38 cm downstream from the nozzle collimate the molecular beam before it enters a 15-cm-long electrostatic deflector. A cut through

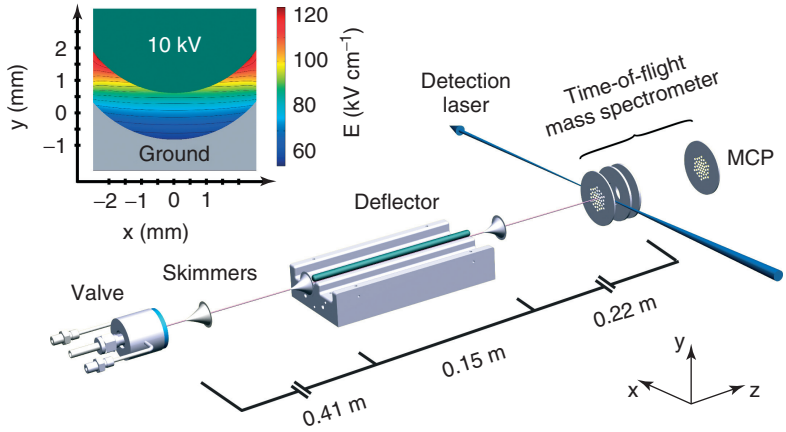

Figure 1.5 Sketch of the experimental setup for electric beam deflection. In the inset, a cut through the deflector is shown, and a contour plot of the electric field strength is given.

the electrodes of the deflector is shown in the inset of Figure 1.5 together with the electric field created. A trough with an inner radius of curvature of 3.2 mm at ground potential and a rod with a radius of 3.0 mm at high voltage create a two-wire field [126]. The vertical gap across the molecular beam axis is 1.4 mm, while the smallest distance between the electrodes is 0.9 mm. The two-wire field geometry is well suited for molecular beam deflection. The gradient of the electric field along the vertical direction is large and nearly constant over a large area explored by the molecular beam, while the electric field is very homogeneous along the horizontal direction. Thus, a polar molecule experiences a nearly constant force in the vertical direction, independent of its position within the deflector, while the force in the horizontal direction (i.e., broadening of the beam in the horizontal direction) is minimized. In our setup, the deflector is mounted such that molecules in high-field-seeking (low-field-seeking) quantum states are deflected upward (downward).

After passing through the deflector, the molecular beam enters the differentially pumped detection chamber via a third skimmer of 1.5 mm diameter. In the detection area, the molecular beam is crossed by one or multiple laser beams which are used to further manipulate or detect the molecules. Using a single focused laser beam that ionizes the molecules, one can measure the vertical profile of the molecular beam by simply moving the laser focus up and down and detecting the relative amounts of ions created. For further experiments the molecule can be aligned using an off-resonant Nd:YAG laser pulse [110] and the degree of alignment can be probed by velocity-map imaging [127] of ionic fragments following multiple-ionization and Coulomb explosion from a ultrashort (fs) laser pulse. The ionic fragments produced in the Coulomb explosion are accelerated in a velocity-focusing geometry toward the detector. The detector can be gated with a time resolution of ~90 ns, which allows mass-selective detection of individual fragments. A microchannel plate

(MCP) detector backed by a phosphor screen is employed to detect the position of mass-selected ions, which serve as the basic observables in the alignment and orientation experiments described in Section 1.4.3.

1.3.2 Alternating-Gradient Focusing

A schematic of the experimental setup for AG focusing of molecules is shown in Figure 1.6. The molecules to be investigated are again seeded in an inert carrier gas and injected through a pulsed valve into vacuum. After passing two skimmers the molecules enter a second, differentially pumped vacuum chamber, where the m/μ-selector is placed. In brief, the selector consists of four polished, 1-m-long cylindrical stainless-steel electrodes of 4 mm diameter. High voltages of 12 kV against ground are applied as shown in Figure 1.6b. The gaps are ∼0.9 mm between two adjacent electrodes and 3.0 mm between two opposing electrodes, resulting in a field strength of 45 kV cm^{-1} on the centerline and a maximum field strength of 135 kV cm^{-1}. Using three high-voltage switches, the field is rapidly switched (< 1 μs) between the two electric field configurations shown in Figure 1.6b. This switching results in the dynamic focusing of neutral molecules. The transmitted molecules are ionized, mass-selected in a time-of-flight mass spectrometer, and subsequently detected using a MCP detector. The molecular beam valve, the high-voltage switching sequences applied to the selector, the detection laser, and the detector are fully synchronized with nanosecond accuracy.

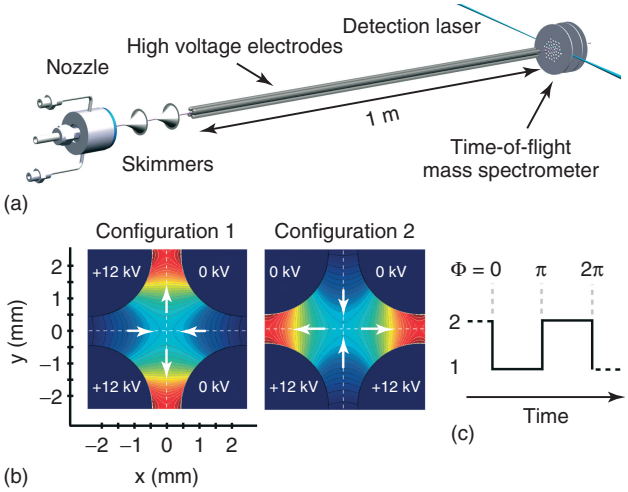

Figure 1.6 Sketch of the experimental setup for alternating gradient focusing, (a) consisting of a pulsed valve, skimmers, the 1-m-long focuser, and time-of-flight mass spectrometer detection setup. (b) Electric field configurations 1 and 2 provide electric saddle point potentials for the molecules that are rotated by 90°. While the molecules are in the focuser, these fields are then rapidly exchanged by the (c) periodic switching function.

1.3.3
Alternating-Gradient Deceleration

In the AG decelerator [72, 91, 92] the long electrodes of the focuser are replaced by many short sections of parallel electrodes. The general scheme of the setup shown in Figure 1.7 is the same as for the focuser. Here, a focuser consisting of 27 pairs of 13-mm-long high-voltage electrodes is shown. In order to obtain the highest possible field strength on the molecular beam axis only two electrodes are used in each stage, and successive stages are mechanically rotated by 90°. The center to center distance of the electrode pairs along the molecular beam axis is 20 mm. If the field is present while the molecules are inside the electrode pair, transverse focusing and defocusing occurs, in analogy to the AG focuser. However, when the molecules fly out of the electrodes into the fringe fields between successive pairs of electrodes, the longitudinal inhomogeneities allow manipulation of the forward velocity, that is, a deceleration of the packet of molecules [91, 93–95].

1.4
Selected Applications

1.4.1
Cluster and Biomolecules Deflection

The electric and magnetic deflection technique has been used extensively since the earliest experiments in the 1920s, see Section 1.2.2. Over the last decade the electric deflection method was improved for the determination of electric susceptibilities

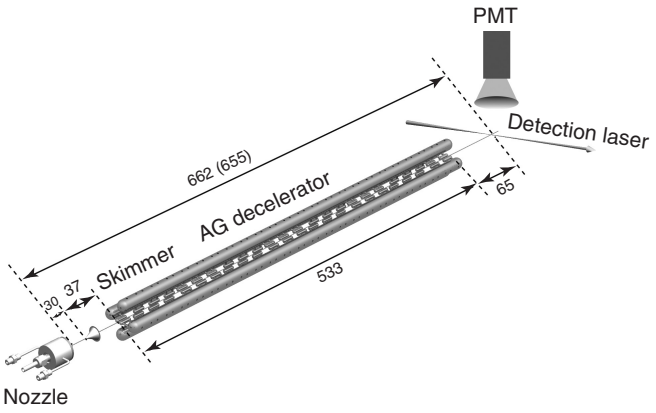

Figure 1.7 Sketch of the experimental setup for alternating gradient deceleration consisting of a pulsed valve, a skimmer, the ∼0.5-m-long decelerator module, and a quantum-state resolving laser-induced-fluorescence detection setup using a photo-multiplier tube (PMT).

of peptides in the gas phase [41, 128] and coupled with mass spectrometry as a first step toward an analytical method for peptide analysis [129].

Electric and magnetic deflection has also proved decisive in cluster research [40, 130]. The method allows investigation of the dipole moments [131] and polarizabilities [132] of various clusters, demonstrating, for example, metallic [133] or ferroelectric [39] behavior for specific samples. Intriguing theoretical structures of alkali metal clusters built onto fullerene molecules have been confirmed through electric deflection experiments [41, 134]. A method to measure AC polarizabilities using the deflection in AC electric fields [98, 99] has been demonstrated for C_{60} molecules [135]. Moreover, in related experiments the combination of an electrostatic deflector and a near-field matter-wave interferometer has been exploited to measure the scalar polarizability of fullerene molecules [136].

In the experiments described in this section the samples are relatively warm ($T \gg 1$ K and $kT \gg B$, with the rotational temperature T and the rotational constant B). Therefore, these experiments operate in a different regime compared to the manipulation experiments described throughout the rest of this chapter. In both cases the deflection of the molecules in the beam is due to their dipole moments in space, that is, along the field direction. For the warm biomolecules and clusters in the deflection experiments this space-fixed dipole moment is due to the polarization of the charge distribution by the electric field, whereas the molecule-fixed dipole moments of the (nearly) freely rotating molecules are averaged to zero, leading to a broadening of the beams, not to a shift. However, for the cold molecular samples in the manipulation experiments, the molecular and the laboratory frame are coupled, since the strong electric fields create oriented – pendular – states. This results in strong deflection forces, because in the pendular states the space-fixed dipole moments are approaching the strengths of the molecule-fixed dipole moments.

1.4.2
Conformer Selection

Spatial separation of conformers can be achieved by exploiting their specific interaction with electric fields. All conformers of a molecule have the same mass and the same connectivities between the atoms (''primary structure''), but often differ in their dipole moments, which are largely determined by the orientations of the functional groups in the molecular frame, that is, by the folding pattern (''secondary structure''). These different dipole moments lead to different Stark shifts of the rotational energy levels in an electric field, as shown in Figure 1.8 for the prototypical large molecule 3-aminophenol (3-AP). The force that a molecule experiences in an electric field is determined by its effective dipole moment μ_{eff}, which is given by the negative slope of the Stark curve. From Figure 1.8 it is obvious that the two conformers of 3-AP will experience different forces in an electric field, which can be exploited to spatially separate them (*vide infra*). This spatial separation of structural isomers has recently been demonstrated by two of the experimental techniques described above, namely using the electric deflector

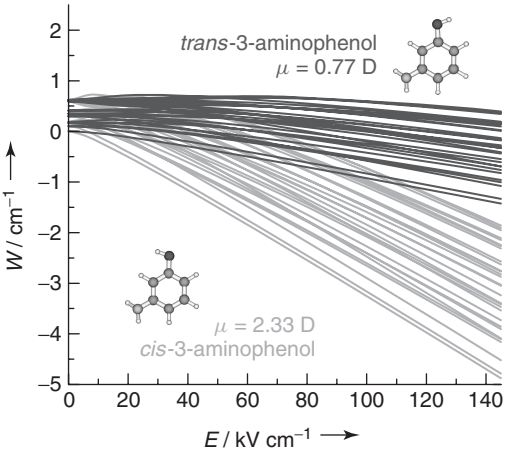

Figure 1.8 Molecular structures, dipole moments, and energies of the lowest rotational states of *cis*- and *trans*-3-aminophenol as a function of the electric field strength. (Reproduced from Ref. [42].)

[42] and, alternatively, using the AG focusing selector [137]. This process – using the electrostatic deflector – is shown schematically in Figure 1.9a. Figure 1.9b shows the experimentally determined vertical molecular beam profiles. From the transmission ratio displayed in the inset, it is obvious that any ratio between the two isomers can be investigated by selecting a sample at the appropriate height. For a laser experiment that can simply be achieved by moving a focusing lens up and down. Generally, one can place an extraction skimmer at the appropriate height to create a pure beam of the desired composition. The deflection approach is the conceptually simplest one. It has the additional advantage that the molecules are separate from the (atomic) seed gas, a point that can be extremely important, for example, for diffraction or reactive scattering experiments, where the excess of the seed gas might obscure all molecular signals. The AG focusing approach, on the other hand, provides active confinement and focusing, and especially also the creation of line foci [137], which could be advantageous for investigations exploiting the long interaction length.

1.4.3
Three-Dimensional Orientation

The quantum-state selection provided by the various manipulation methods can even be exploited for further control experiments. As described in Box 1.3 the most polar states are, in general terms, the lowest rotational states, and one can thus create a sample of these lowest/most polar states using the methods described in this chapter. These states, at the same time, are the states that have the largest effective polarizabilities and, therefore, can be aligned (using AC fields) [119] or oriented (using DC fields) especially well. In order to completely fix complex molecules

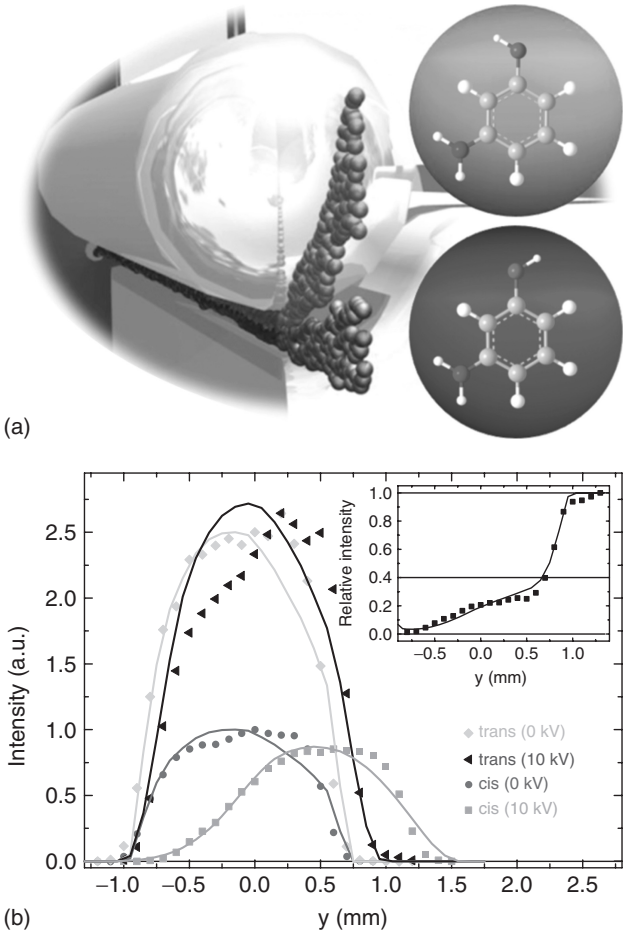

Figure 1.9 (a) Conformer separation by deflection. (Reproduced from Ref. [42].) The sketch on the left illustrates the spatial separation of the conformers of 3-aminophenol in a molecular beam entering the device through a skimmer from the back. The figure on the right shows an actual measurement of the vertical beam profiles. (b) These profiles can be independently obtained, for example, through resonance-enhanced multiphoton ionization, which spectrally discriminates the two species. The inset shows the relative abundance of the *trans*-conformer as a function of vertical position in the deflected molecular beam.

in space – which are three-dimensional objects – one has to three-dimensionally orient them. One-dimensional orientation is readily achieved for polar molecules using the brute-force approach [103, 104]. Three-dimensional alignment was demonstrated a decade ago using elliptically polarized AC (laser) fields [138]. However, until recently it was not possible to fully, three-dimensionally, orient ensembles of molecules in space. The selection of the lowest rovibronic states of the prototypical 2,6-difluoroiodobenzene molecule has allowed strong 3D orientation

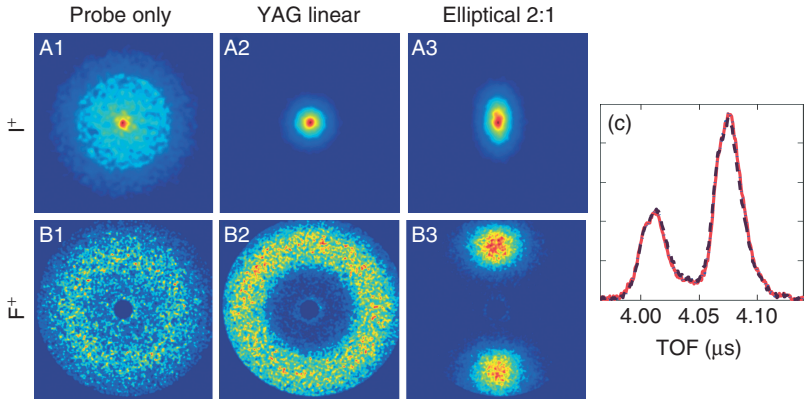

Figure 1.10 Velocity-map images (A1–B3) and time-of-flight distributions (C) of difluoroiodobenzene. Images A1–A3 show the velocity distribution of iodine ions, B1–B3 of fluorine ions for isotropic (A1, B1), 1D-oriented (A2, B2) and 3D oriented (A3, B3) difluoroiodobenzene molecules. The scales of these images can be calibrated by calculation of the Coulomb repulsion force in the fragmenting molecule, but these scales are not relevant for the discussion of alignment and orientation. The time-of-flight distribution of iodine ions represents the forward–backward asymmetry of the 3D-oriented sample. (Reproduced from Ref. [120].)

using the mixed (AC and DC) field approach, originally described for the 1D case by Friedrich and Herschbach [112]. In Figure 1.10 the ion-momentum distributions of I^+ and F^+ following Coulomb explosion are shown for three different experimental conditions. These fragment ion distributions provide a direct measurement of the C–I and C–F bonds in the intact molecule before Coulomb explosion. In all cases, the experiments are performed on a quantum-state selected ensemble containing some 10 rotational states. The first column shows the ion distributions for an isotropic sample, in which the molecules are oriented arbitrarily in space. When one aligns and orients the molecules one-dimensionally along the detector normal, one obtains a very sharp peak of I^+ ions at the center of the detector, and a ring of F^+ ions. This demonstrates the strong degree of 1D orientation along the laser polarization axis and, on the other hand, the free rotation of the molecules about that axis. The orientation is proved by the asymmetry of the arrival time-distribution of molecules at the detector (Figure 1.10c). If one uses 2 : 1 elliptically polarized light with the long axis of the polarization ellipse along the detector normal, the 1D orientation is slightly weaker in the vertical direction, as observed in the I^+ images. However, from the F^+ images it is clear that the molecule is now fully fixed in space.

1.4.4
Molecular-Frame Photoelectron Angular Distributions

The controlled samples provided by the techniques described here allow the measurement of molecular properties directly in the molecular frame. This includes,

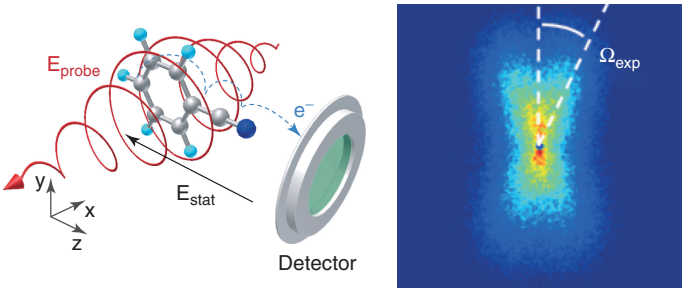

Figure 1.11 Molecular-frame photoelectron-angular-distribution imaging schematics (a) and the corresponding molecular-frame photoelectron angular distribution of 3D oriented benzonitrile molecules (b); [121] (see text for details).

for example, the investigation of electronic properties directly in the molecular frame. Figure 1.11a gives a schematic view of the corresponding experiment [121]. Benzonitrile molecules are fixed in space in a vertical plane perpendicular to the detector. The 3D molecules are ionized with a strong (1.2×10^{14} W cm^{-2}) non-resonant (800 nm) ultrashort (25 fs) left-circularly polarized laser pulse, resulting in single ionization of benzonitrile molecules. The detector is operated such that it projects the electron momentum onto the position-sensitive detector and the resulting images are recorded. The major features in the resulting image, shown in Figure 1.11b, are the up–down asymmetry and the four "lobes" at an angle $\Omega = 18^{\circ}$. The former can readily be understood in terms of the differences in the Stark effects of the neutral molecule and the created ion [118]. The latter is a direct image of the density of the highest occupied orbitals, from which the electron is ejected [122].

These experiments hold strong promises for the investigation of ultrafast molecular and chemical dynamics, as demonstrated in first benchmark experiments on the rotational dynamics of napthalene [139]. Investigating dynamics of the controlled samples with vacuum ultraviolet or X-ray single-photon-ionization photoelectron imaging techniques [140] could provide even further details on the electronic structure and the molecular dynamics. Furthermore, these controlled molecular samples provide unique opportunities to investigate stereochemistry in the reactions of isolated and well-defined molecules, promising direct experimental proofs or falsifications of the often still statistically derived – yet conceptually so powerful – reaction mechanisms in chemistry.

1.5 Conclusions and Perspectives

Using static inhomogeneous electric fields, complex polar molecules can be deflected and spatially dispersed according to their effective dipole moment, that is, according to their quantum state. Using switched electric fields one can also actively

focus or even decelerate packets of molecules in a small set of quantum states. Both approaches, deflection and focusing, can be used to prepare packets of individual structural isomers of such complex molecules. Moreover, because the methods intrinsically create very polar samples, these molecular ensembles can be aligned and oriented extremely well. Overall, these techniques allow one to prepare packets of individual structural isomers that are all fixed in space due to large degrees of alignment and orientation. In addition, the electric deflection allows complete separation of the molecular ensemble from the atomic seed gas, resulting in pure molecular samples. Experiments aimed at recording the ''molecular movie'' will strongly benefit from these controlled samples. This includes experiments on molecular frame photoelectron angular distributions [121, 140, 141], as described above, photoelectron holography [142–144], high-harmonic generation and molecular orbital tomography [23], or ultrafast X-ray [1, 145] or electron diffraction [24, 25].

Acknowledgments

The research described here strongly benefitted from many discussions within the Department of Molecular Physics at the Fritz Haber Institute in Berlin and the Stapelfeldt group at Aarhus University. The expert technical support at the FHI was crucial for the implementation and demonstration of the methods described herein. Early parts of this work were supported by the DFG in priority program 1116.

References

1. Filsinger, F., Meijer, G., Stapelfeldt, H., Chapman, H., and Küpper, J. (2011) *Phys. Chem. Chem. Phys.*, **13**, 2076.
2. Ospelkaus, S., Ni, K., Wang, D., Miranda, M.D., Neyenhuis, B., Quéméner, G., Julienne, P., Bohn, J., Jin, D., and Ye, J. (2010) *Science*, **327**, 853.
3. Ni, K.K., Ospelkaus, S., Wang, D., Quéméner, G., Neyenhuis, B., de Miranda, M.H.G., Bohn, J.L., Ye, J., and Jin, D.S. (2010) *Nature*, **464**, 1324.
4. de Miranda, M.H.G., Chotia, A., Neyenhuis, B., Wang, D., Quéméner, G., Ospelkaus, S., Bohn, J.L., Ye, J., and Jin, D.S. (2011) *Nat. Phys.* **7**, 502.
5. Gilijamse, J.J., Hoekstra, S., van de Meerakker, S.Y.T., Groenenboom, G.C., and Meijer, G. (2006) *Science*, **313**, 1617.
6. Scharfenberg, L., Kos, J., Dagdigian, P.J., Alexander, M.H., Meijer, G., and van de Meerakker, S.Y.T. (2010) *Phys. Chem. Chem. Phys.*, **12**, 10660.
7. Remacle, F. and Levine, R. (2006) *Proc. Natl. Acad. Sci.*, **103**, 6793.
8. Weinkauf, R., Schermann, J.-P., de Vries, M.S., and Kleinermanns, K. (2002) *Eur. Phys. J. D*, **20** (3), 309–626.
9. Bio-active molecules in the gas phase (2004) *Phys. Chem. Chem. Phys.*, **6**, 2543.
10. de Vries, M.S. and Hobza, P. (2007) *Annu. Rev. Phys. Chem.*, **58**, 585.
11. Kim, S.K., Lee, W., and Herschbach, D.R. (1996) *J. Phys. Chem.*, **100**, 7933.
12. Piuzzi, F., Mons, M., Dimicoli, I., Tardivel, B., and Zhao, Q. (2001) *Chem. Phys.*, **270**, 205.
13. Suenram, R.D. and Lovas, F.J. (1980) *J. Am. Chem. Soc.*, **102**, 7180.
14. Rizzo, T.R., Park, Y.D., Peteanu, L., and Levy, D.H. (1985) *J. Chem. Phys.*, **83**, 4819.

15. Nir, E., Kleinermanns, K., and de Vries, M.S. (2000) *Nature*, **408**, 949.
16. Snoek, L.C., Robertson, E.G., Kroemer, R.T., and Simons, J.P. (2000) *Chem. Phys. Lett.*, **321**, 49.
17. Bakker, J.M., Aleese, L.M., Meijer, G., and von Helden, G. (2003) *Phys. Rev. Lett.*, **91**, 203003.
18. Dong, F. and Miller, R.E. (2002) *Science*, **298**, 1227.
19. Lesarri, A., Cocinero, E.J., Lopez, J.C., and Alonso, J.L. (2004) *Angew. Chem. Int. Ed.*, **43**, 605.
20. Reese, J.A., Nguyen, T.V., Korter, T.M., and Pratt, D.W. (2004) *J. Am. Chem. Soc.*, **126**, 11387.
21. Filsinger, F., Wohlfart, K., Schnell, M., Grabow, J.-U., and Küpper, J. (2008) *Phys. Chem. Chem. Phys.*, **10**, 666.
22. Dian, B.C., Clarkson, J.R., and Zwier, T.S. (2004) *Science*, **303**, 1169.
23. Itatani, J., Levesque, J., Zeidler, D., Niikura, H., Pépin, H., Kieffer, J.C., Corkum, P.B., and Villeneuve, D.M. (2004) *Nature*, **432**, 867.
24. Williamson, J.C., Cao, J.M., Ihee, H., Frey, H., and Zewail, A.H. (1997) *Nature*, **386**, 159.
25. Siwick, B.J., Dwyer, J.R., Jordan, R.E., and Miller, R.J.D. (2003) *Science*, **302**, 1382.
26. Chapman, H.N., Barty, A., Bogan, M.J., Boutet, S., Frank, S., Hau-Riege, S.P., Marchesini, S., Woods, B.W., Bajt, S., Benner, W.H., and Plönjes, E., London, R.A. *et al.* (2006) *Nat. Phys.*, **2**, 839.
27. von Helden, G., Wyttenbach, T., and Bowers, M.T. (1995) *Science*, **267**, 1483.
28. Jarrold, M. (2007) *Phys. Chem. Chem. Phys.*, **9**, 1659.
29. Dian, B.C., Longarte, A., and Zwier, T.S. (2002) *Science*, **296**, 2369.
30. Erlekam, U., Frankowski, M., von Helden, G., and Meijer, G. (2007) *Phys. Chem. Chem. Phys.*, **9**, 3786.
31. Dunoyer, L. (1911) *C. R. Hebd. Seances Acad. Sci. (Fr.)*, **152**, 592.
32. Stern, O. (1921) *Z. Phys.*, **7**, 249.
33. Gerlach, W. and Stern, O. (1922) *Z. Phys.*, **9**, 349.
34. Kallmann, H. and Reiche, F. (1921) *Z. Phys.*, **6**, 352.
35. Wrede, E. (1927) *Z. Phys.*, **44**, 261.
36. Stern, O. (1926) *Z. Phys.*, **39**, 751.
37. Rabi, I.I., Zacharias, J.R., Millman, S., and Kusch, P. (1938) *Phys. Rev.*, **53**, 318.
38. Rabi, I.I., Millman, S., Kusch, P., and Zacharias, J.R. (1939) *Phys. Rev.*, **55**, 526.
39. Moro, R., Xu, X., Yin, S., and de Heer, W.A. (2003) *Science*, **300**, 1265.
40. de Heer, W.A. and Kresin, V.V. (2010) Electric and magnetic dipole moments of free nanoclusters, *Handbook of Nanophysics* (ed. Sattler, K.D.), CRC Press, arXiv:0901.4810.
41. Broyer, M., Antoine, R., Compagnon, I., Rayane, D., and Dugourd, P. (2007) *Phys. Scr.*, **76**, C135.
42. Filsinger, F., Küpper, J., Meijer, G., Hansen, J.L., Maurer, J., Nielsen, J.H., Holmegaard, L., and Stapelfeldt, H. (2009) *Angew. Chem. Int. Ed.*, **48**, 6900.
43. Friedburg, H. and Paul, W. (1951) *Naturwissenschaften*, **38**, 159.
44. Bennewitz, H.G. and Paul, W. (1954) *Z. Phys.*, **139**, 489.
45. Bennewitz, H.G., Paul, W., and Schlier, C. (1955) *Z. Phys.*, **141**, 6.
46. Gordon, J.P., Zeiger, H.J., and Townes, C.H. (1954) *Phys. Rev.*, **95**, 282.
47. Gordon, J.P., Zeiger, H.J., and Townes, C.H. (1955) *Phys. Rev.*, **99**, 1264.
48. Bennewitz, H.G., Kramer, K.H., Toennies, J.P., and Paul, W. (1964) *Z. Phys.*, **177**, 84.
49. Brooks, P.R. and Jones, E.M. (1966) *J. Chem. Phys.*, **45**, 3449.
50. Beuhler, R.J., Bernstein, R.B., and Kramer, K.H. (1966) *J. Am. Chem. Soc.*, **88**, 5331.
51. Stolte, S. (1982) *Ber. Bunsen-Ges. Phys. Chem.*, **86**, 413.
52. Stolte, S. (1988) in *Atomic and Molecular Beam Methods*, (ed. G. Scholes), vol. 1, Chapter 25, Oxford University Press, New York, pp. 631–652.
53. Parker, D.H. and Bernstein, R.B. (1989) *Annu. Rev. Phys. Chem.*, **40**, 561.
54. Kuipers, E.W., Tenner, M.G., Kleyn, A., and Stolte, S. (1988) *Nature*, **334**, 420.
55. Rakitzis, T.P., van den Brom, A.J., and Janssen, M.H.M. (2004) *Science*, **303**, 1852.
56. Bethlem, H.L., Berden, G., and Meijer, G. (1999) *Phys. Rev. Lett.*, **83**, 1558.

57. Crompvoets, F.M.H., Bethlem, H.L., Jongma, R.T., and Meijer, G. (2001) *Nature*, **411**, 174.

58. Bethlem, H.L., Berden, G., Crompvoets, F.M.H., Jongma, R.T., van Roij, A.J.A., and Meijer, G. (2000) *Nature*, **406**, 491.

59. van Veldhoven, J., Bethlem, H.L., and Meijer, G. (2005) *Phys. Rev. Lett.*, **94**, 083001.

60. Meek, S.A., Conrad, H., and Meijer, G. (2009) *Science*, **324**, 1699.

61. van de Meerakker, S.Y.T., Bethlem, H.L., and Meijer, G. (2008) *Nat. Phys.*, **4**, 595.

62. Bell, M.T., and Softley, T.P. (2009) *Mol. Phys.*, **107**, 99.

63. van de Meerakker, S.Y.T., Bethlem, H.L., and Meijer, G. (2009) *Cold Molecules: Theory, Experiment, Applications*, Chapter 14, CRC Press, Taylor&Francis Group.

64. Schnell, M. and Meijer, G. (2009) *Angew. Chem. Int. Ed.*, **48**, 6010.

65. Ketterle, W. and Pritchard, D.E. (1992) *Appl. Phys. B*, **54**, 403.

66. Wing, W.H. (1984) *Prog. Quant. Electr.*, **8**, 181.

67. Courant, E.D. and Snyder, H.S. (1958) *Ann. Phys.*, **3**, 1.

68. Courant, E.D., Livingston, M.S., and Snyder, H.S. (1952) *Phys. Rev.*, **88**, 1190.

69. Paul, W. (1990) *Rev. Mod. Phys.*, **62**, 531.

70. Paul, W. and Steinwedel, H. (1953) *Z. Naturforsch. A*, **8**, 448.

71. Paul, W., Osberghaus, O., and Fischer, E. (1958) Forschungsbericht, Wirtschafts- und Verkehrministerium Nordrhein Westfalen.

72. Auerbach, D., Bromberg, E.E.A., and Wharton, L. (1966) *J. Chem. Phys.*, **45**, 2160.

73. Kakati, D. and Lainé, D.C. (1967) *Phys. Lett. A*, **24**, 676.

74. Kakati, D. and Lainé, D.C. (1969) *Phys. Lett. A*, **28**, 786.

75. Kakati, D. and Lainé, D.C. (1971) *J. Phys. E*, **4**, 269.

76. Günther, F. and Schügerl, K. (1972) *Z. Phys. Chem.*, **NF 80**, 155.

77. Lübbert, A., Günther, F., and Schügerl, K. (1975) *Chem. Phys. Lett.*, **35**, 210.

78. Lübbert, A., Rotzoll, G., and Günther, F. (1978) *J. Chem. Phys.*, **69**, 5174.

79. Junglen, T., Rieger, T., Rangwala, S.A., Pinkse, P.W.H., and Rempe, G. (2004) *Phys. Rev. Lett.*, **92**, 223001.

80. Wall, T.E., Armitage, S., Hudson, J.J., Sauer, B.E., Dyne, J.M., Hinds, E.A., and Tarbutt, M.R. (2009) *Phys. Rev. A*, **80**, 043407.

81. Putzke, S., Filsinger, F., Haak, H., Küpper, J., and Meijer, G. (2011) *Phys. Chem. Chem. Phys.*, **13**, 18962–18970, DOI: 10.1039/C1CP20721K.

82. Al-Amiedy, D.H.H. and Lainé, D.C. (1978) *Phys. Lett. A*, **66**, 94.

83. Lainé, D.C. and Sweeting, R. (1971) *Phys. Lett. A*, **34**, 144.

84. Helmer, J.C., Jacobus, F.B., and Sturrock, P.A. (1960) *J. Appl. Phys.*, **31**, 458.

85. Chien, K.-R., Foreman, P.B., Castleton, K.H., and Kukolich, S.G. (1975) *Chem. Phys.*, **7**, 161.

86. Loesch, H.-J. (1996) *Chem. Phys.*, **207**, 427.

87. Loesch, H.J. and Scheel, B. (2000) *Phys. Rev. Lett.*, **85**, 2709.

88. Wolfgang, R. (1968) *Sci. Am.*, **219**, 44.

89. Bromberg, E.E.A. (1972) Acceleration and alternate-gradient focusing of neutral polar diatomic molecules, PhD thesis, University of Chicago, Chicago, IL, USA.

90. Golub, R. (1967) On decelerating molecules, PhD thesis, Massachusetts Institute of Technology, Cambridge, MA, USA.

91. Bethlem, H.L., van Roij, A.J.A., Jongma, R.T., and Meijer, G. (2002) *Phys. Rev. Lett.*, **88**, 133003.

92. Bethlem, H.L., Tarbutt, M.R., Küpper, J., Carty, D., Wohlfart, K., Hinds, E.A., and Meijer, G. (2006) *J. Phys. B*, **39**, R263.

93. Tarbutt, M.R., Bethlem, H.L., Hudson, J.J., Ryabov, V.L., Ryzhov, V.A., Sauer, B.E., Meijer, G., and Hinds, E.A. (2004) *Phys. Rev. Lett.*, **92**, 173002.

94. Wohlfart, K., Grätz, F., Filsinger, F., Haak, H., Meijer, G., and Küpper, J. (2008) *Phys. Rev. A*, **77**, 031404(R).

95. Wohlfart, K., Filsinger, F., Grätz, F., Küpper, J., and Meijer, G. (2008) *Phys. Rev. A*, **78**, 033421.

96. Wohlfart, K. (2008) Alternating-gradient focusing and deceleration of large molecules, Dissertation, Free University, Berlin, Germany.

97. Bethlem, H.L., van Veldhoven, J., Schnell, M., and Meijer, G. (2006) *Phys. Rev. A*, **74**, 063403.

98. Stapelfeldt, H., Sakai, H., Constant, E., and Corkum, P.B. (1997) *Phys. Rev. Lett.*, **79**, 2787.

99. Zhao, B.S., Chung, H.S., Cho, K., Lee, S.H., Hwang, S., Yu, J., Ahn, Y.H., Sohn, J.Y., Kim, D.S., Kang, W.K., and Chung, D.S. (2000) *Phys. Rev. Lett.*, **85**, 2705.

100. Fulton, R., Bishop, A.I., and Barker, P.F. (2004) *Phys. Rev. Lett.*, **93**, 243004.

101. Enomoto, K. and Momose, T. (2005) *Phys. Rev. A*, **72**, 061403.

102. Odashima, H., Merz, S., Enomoto, K., Schnell, M., and Meijer, G. (2010) *Phys. Rev. Lett.*, **104**, 253001.

103. Loesch, H.J. and Remscheid, A. (1990) *J. Chem. Phys.*, **93**, 4779.

104. Friedrich, B. and Herschbach, D.R. (1991) *Nature*, **353**, 412.

105. Loesch, H.J. (1995) *Annu. Rev. Phys. Chem.*, **46**, 555.

106. Kong, W. (2001) *Int. J. Mod. Phys. B*, **15**, 3471.

107. Castle, K.J. and Kong, W. (2000) *J. Chem. Phys.*, **112**, 10156.

108. Reuss, J. (1988) in *Atomic and Molecular Beam Methods* (ed. G. Scholes), vol. 1, Chapter 11, Oxford University Press, New York, pp. 276–292.

109. Orr-Ewing, A.J. and Zare, R.N. (1994) *Annu. Rev. Phys. Chem.*, **45**, 315.

110. Stapelfeldt, H. and Seideman, T. (2003) *Rev. Mod. Phys.*, **75**, 543.

111. Seideman, T. and Hamilton, E. (2005) *Adv. At. Mol. Opt. Phys.*, **52**, 289.

112. Friedrich, B. and Herschbach, D. (1999) *J. Chem. Phys.*, **111**, 6157.

113. Friedrich, B. and Herschbach, D. (1999) *J. Phys. Chem. A*, **103**, 10280.

114. Minemoto, S., Nanjo, H., Tanji, H., Suzuki, T., and Sakai, H. (2003) *J. Chem. Phys.*, **118**, 4052.

115. Buck, U. and Fárník, M. (2006) *Int. Rev. Phys. Chem.*, **25**, 583.

116. Goban, A., Minemoto, S., and Sakai, H. (2008) *Phys. Rev. Lett.*, **101**, 013001.

117. Ghafur, O., Rouzee, A., Gijsbertsen, A., Siu, W.K., Stolte, S., and Vrakking, M.J.J. (2009) *Nat. Phys.*, **5**, 289.

118. Dimitrovski, D., Abu-samha, M., Madsen, L.B., Filsinger, F., Meijer, G., Küpper, J., Holmegaard, L., Kalhøj, L., Nielsen, J.H., and Stapelfeldt, H. (2011) *Phys. Rev. A*, **83**, 023405.

119. Holmegaard, L., Nielsen, J.H., Nevo, I., Stapelfeldt, H., Filsinger, F., Küpper, J., and Meijer, G. (2009) *Phys. Rev. Lett.*, **102**, 023001.

120. Nevo, I., Holmegaard, L., Nielsen, J.H., Hansen, J.L., Stapelfeldt, H., Filsinger, F., Meijer, G., and Küpper, J. (2009) *Phys. Chem. Chem. Phys.*, **11**, 9912.

121. Holmegaard, L., Hansen, J.L., Kalhøj, L., Kragh, S.L., Stapelfeldt, H., Filsinger, F., Küpper, J., Meijer, G., Dimitrovski, D., Abu-samha, M., Martiny, C.P.J., and Madsen, L.B. (2010) *Nat. Phys.*, **6**, 428.

122. Hansen, J.L., Holmegaard, L., Kalhøj, L., Kragh, S.L., Stapelfeldt, H., Filsinger, F., Küpper, J., Meijer, G., Dimitrovski, D., Abu-samha, M., Martiny, C.P.J., and Madsen, L.B. (2011) *Phys. Rev. A*, **83**, 023406.

123. Kumarappan, V., Bisgaard, C.Z., Viftrup, S.S., Holmegaard, L., and Stapelfeldt, H. (2006) *J. Chem. Phys.*, **125**, 194309.

124. Hillenkamp, M., Keinan, S., and Even, U. (2003) *J. Chem. Phys.*, **118**, 8699.

125. Even, U., Jortner, J., Noy, D., Lavie, N., and Cossart-Magos, N. (2000) *J. Chem. Phys.*, **112**, 8068.

126. Ramsey, N.F. (1956) *Molecular Beams, The International Series of Monographs on Physics* Oxford University Press, London, GB (reprinted in Oxford Classic Texts in the Physical Sciences, 2005).

127. Eppink, A.T.J.B. and Parker, D.H. (1997) *Rev. Sci. Instrum.*, **68**, 3477.

128. Antoine, R., Compagnon, I., Rayane, D., Broyer, M., Dugourd, P., Breaux, G., Hagemeister, F.C., Pippen, D., Hudgins, R.R., and Jarrold, M.F. (2002) *J. Am. Chem. Soc.*, **124**, 6737.

129. Antoine, R., Compagnon, I., Rayane, D., Broyer, M., Dugourd, P., Sommerer, N., Rossignol, M., Pippen, D., Hagemeister, F.C., and Jarrold, M.F. (2003) *Anal. Chem.*, **75**, 5512.

130. Becker, J.A. (1997) *Angew. Chem. Int. Ed.*, **36**, 1391.

131. Schäfer, S., Assadollahzadeh, B., Mehring, M., Schwerdtfeger, P., and Schäfer, R. (2008) *J. Phys. Chem. A*, **112**, 12312.

132. Tarnovsky, V., Bunimovicz, M., Vuskovic, L., Stumpf, B., and Bederson, B. (1993) *J. Chem. Phys.*, **98**, 3894.

133. Bowlan, J., Liang, A., and de Heer, W.A. (2011) *Phys Rev Lett*, **106**, 043401.

134. Rabilloud, F., Antoine, R., Broyer, M., Compagnon, I., Dugourd, P., Rayane, D., and Calvo, F. (2007) *J. Phys. Chem. C*, **111**, 17795.

135. Ballard, A., Bonin, K., and Louderback, J. (2000) *J. Chem. Phys.*, **113**, 5732.

136. Berninger, M., Stefanov, A., Deachapunya, S., and Arndt, M. (2007) *Phys. Rev. A*, **76**, 013607.

137. Filsinger, F., Erlekam, U., von Helden, G., Küpper, J., and Meijer, G. (2008) *Phys. Rev. Lett.*, **100**, 133003.

138. Larsen, J.J., Hald, K., Bjerre, N., Stapelfeldt, H., and Seideman, T. (2000) *Phys. Rev. Lett.*, **85**, 2470.

139. Hansen, J., Stapelfeldt, H., Dimitrovski, D., Abu-Samha, M., Martiny, C., and Madsen, L. (2011) *Phys. Rev. Lett.*, **106**, 073001.

140. Landers, A., Weber, T., Ali, I., Cassimi, A., Hattass, M., Jagutzki, O., Nauert, A., Osipov, T., Staudte, A., Prior, M., Schmidt-Böcking, H., Cocke, C. *et al.* (2001) *Phys. Rev. Lett.*, **87**, 013002.

141. Nugent-Glandorf, L., Scheer, M., Samuels, D., Mulhisen, A., Grant, E., Yang, X., Bierbaum, V., and Leone, S. (2001) *Phys. Rev. Lett.*, **87**, 193002.

142. Szöke, A. (1986) *AIP Conf. Proc.*, **147**, 361.

143. Barton, J.J. (1988) *Phys. Rev. A*, **61**, 1356.

144. Krasniqi, F., Najjari, B., Strüder, L., Rolles, D., Voitkiv, A., and Ullrich, J. (2010) *Phys. Rev. A*, **81**, 033411.

145. Neutze, R., Wouts, R., van der Spoel, D., Weckert, E., and Hajdu, J. (2000) *Nature*, **406**, 752.

146. Fenn, J.B. (1996) *Annu. Rev. Phys. Chem.*, **47**, 1.

147. Gordy, W. and Cook, R.L. (1984) *Microwave Molecular Spectra*, 3rd edn, John Wiley & Sons, Inc., New York.

148. Wohlfart, K., Schnell, M., Grabow, J.-U., and Küpper, J. (2008) *J. Mol. Spec.*, **247**, 119.

149. Küpper, J., Filsinger, F., and Meijer, G. (2009) *Faraday Disc.*, **142**, 155.